Supporting Information for

Selenidostannates and a silver-selenidostannate synthesized in deep eutectic solvents: crystal structures and thermochromic study

Kai-Yao Wang,[,†] Hua-Wei Liu,[†] Shu Zhang,[†] Dong Ding,[†] Lin Cheng,[§] Cheng Wang*[,†]*

[†]Institute for New Energy Materials and Low-Carbon Technologies, School of Materials Science and Engineering, Tianjin Key Laboratory of Advanced Functional Porous Materials, Tianjin University of Technology, Tianjin 300384, P. R. China.

[§]College of Chemistry, Tianjin Normal University, Tianjin 300387, P. R. China.

1. Tables

Table S1 Summary of the $[Sn_3Se_7]_n^{2n-}$ layer-containing compounds in the literature and their band gaps and structural types.

Compound	Space group	Band gap	Type	Ref.
$Cs_2Sn_3Se_7$	*C*2/*c*	NA	I	[1]
$[enH_2][Sn_3Se_7]\cdot 0.5en$	*Fdd*2	NA	II	[2]
$(TMA)_2Sn_3Se_7$	$P2_12_12_1$	2.12 eV	III	[3]
$(C_7N_4OH_{16})_2Sn_3Se_7\cdot H_2$	*Pbca*	NA	III	[4]
$[(C_2H_5)_3NH]_2Sn_3Se_7\cdot 0.25H_2O$	$P2_1/n$	2.1 eV	III	[5]
$(NH_3(CH_2)_8NH_3)Sn_3Se_7$	$P\bar{1}$	NA	II	[6]
$(NH_3(CH_2)_{10}NH_3)Sn_3Se_7$	*C*2/*c*	NA	II	[6]
$[Mn(peha)][Sn_3Se_7]$	$P2_1/n$	NA	III	[7]
$[Fe(phen)_3]_n(Sn_3Se_7)_n\cdot 1.25nH_2O$	$R\bar{3}c$	1.97 eV	II	[8]
$[prmmim]_2[Sn_3Se_7]$	$P322_1$	NA	II	[9]
$[bmmim]_2[Sn_3Se_7]$	$P322_1$	2.2 eV	II	[9]
$[DBNH]_2[Sn_3Se_7]\cdot PEG$	*C*2/*c*	2.13 eV	I	[10]
$[DBNH]_3[NH_4][Sn_6Se_{14}]$	$R\bar{3}$	2.02 eV	I	[10]
$[Mn(dien)_2]Sn_3Se_7\cdot 0.5H_2O$	$P2_1/n$	1.89 eV	III	[11]
$[Fe(tatda)]Sn_3Se_7$	$P2_1/n$	1.93 eV	II	[11]
$[Mn(en)_{2.5}(en\text{-}Me)_{0.5}][Sn_3Se_7]$	$P2_1/c$	NA	III	[12]
$[Mn(en)_3]Sn_3Se_7$	$P2_1/n$	1.99 eV	III	[13]
$[Mn(dien)_2]Sn_3Se_7\cdot H_2O$	$P2_1/n$	2.04 eV	III	[13]
$(H^+\text{-}DBN)_2[Sn_3Se_7]$	$Cmc2_1$	2.02 eV	II	[14]
$[(CH_3)_3N(CH_2)_2OH]_2[Sn_3Se_7]\cdot H_2O$	$P2_1/n$	NA	III	[15]
$[(CH_3)_3N(CH_2)_2CH_3]_2[Sn_3Se_7]$	*Pbca*	2.35 eV	III	[15]
$(BuMe_3N)_2[Sn_3Se_7]$	*C*2/*c*	NA	I	[16]

Table S2 Summary of the Ag-Sn-Se compounds and their band gaps in the literature.

Compound	Space group	Band gap	Ref.
$K_2Ag_2SnSe_4$	*P*2/*c*	1.8 eV	[17]
$K_2Ag_2Sn_2Se_6$	*P*4/*mcc*	NA	[18]
β-Ag_8SnSe_6	$Pmn2_1$	NA	[19]
$BaAg_2SnSe_4$	*I*222	0.2 eV	[20]
$La_3AgSnSe_7$	$P6_3$	NA	[21]
$A_3AgSn_3Se_8$ (A = Rb, K)	*P*4/*nbm*	1.8 eV	[22]
$K_3AgSn_3Se_8$	*P*4/*nbm*	1.8 eV	[23]
$[(Me)_2NH_2]_{0.75}[Ag_{1.25}SnSe_3]$	$P\bar{4}2_1m$	1.85 eV	[24]
$[bmmim]_7[AgSn_{12}Se_{28}]$	$P\bar{1}$	2.2 eV	[25]
$(NH_4)_4Ag_{12}Sn_7Se_{22}$	*C*2/*c*	1.21 eV	[26]
$[CH_3NH_3]_2[H_3O]Ag_5Sn_4Se_{12}\cdot C_2H_5OH$	$P\bar{4}2_1m$	1.80 eV	[27]

2. Figures

2.1 Synthesis

Compound 1:

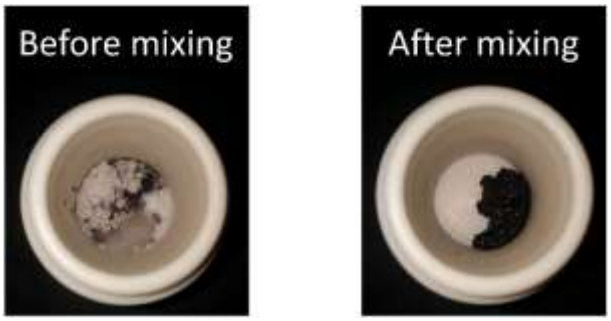

Figure S1. Photographs of the reactants, i.e. Sn, Se, $[NH_2(CH_3)_2]Cl$, urea (without $N_2H_4{\cdot}H_2O$), before and after being mixed for the synthesis of compound **1**. The transforming from bulk solid reactants to a viscous liquid mixture after being stirred indicates the formation of $[NH_2(CH_3)_2]Cl$-urea DES.

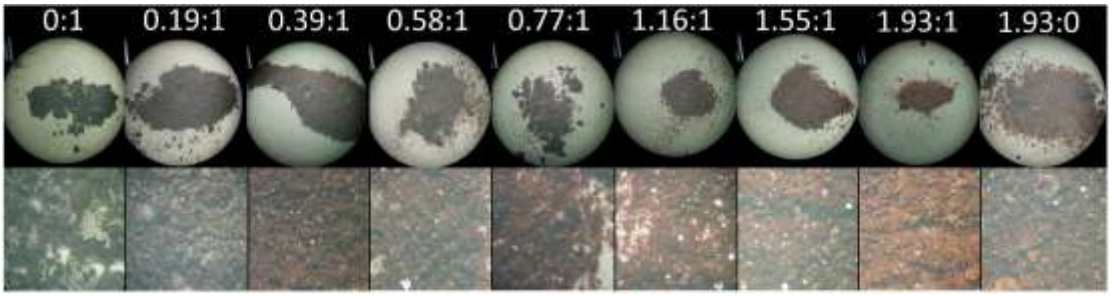

Figure S2. Photographs of the products obtained from the optimizing reactions for **1** with different $N_2H_4{\cdot}H_2O$:urea molar ratios at 160 °C. Top line: products washed by distilled water; bottom line: magnified imaging of the products.

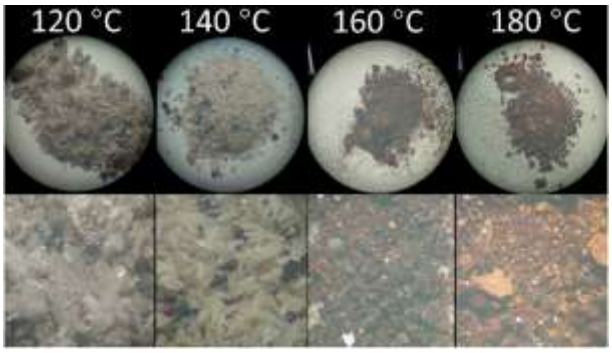

Figure S3. Photographs of the products obtained from the optimizing reactions for **1** ($N_2H_4{\cdot}H_2O$:urea = 0.58:1) performed at different temperatures. Top line: products washed by distilled water; bottom line: magnified imaging of the products.

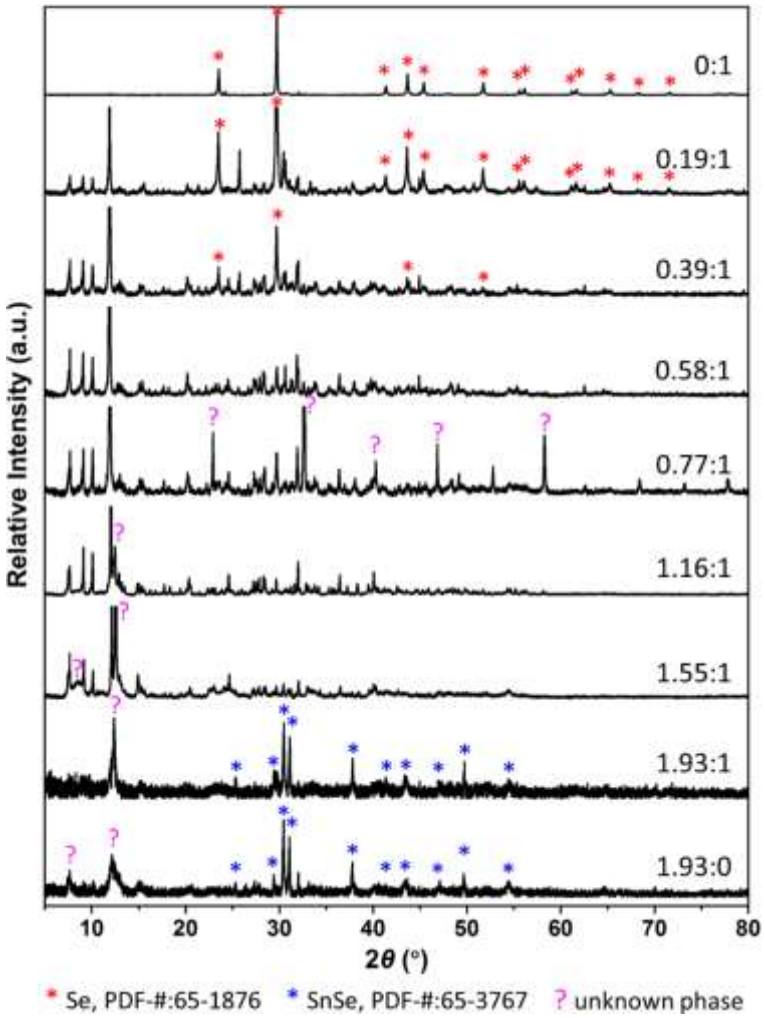

Figure S4. Powder XRD patterns for the products from optimizing reactions for **1** with different $N_2H_4 \cdot H_2O$:urea ratio at 160 °C.

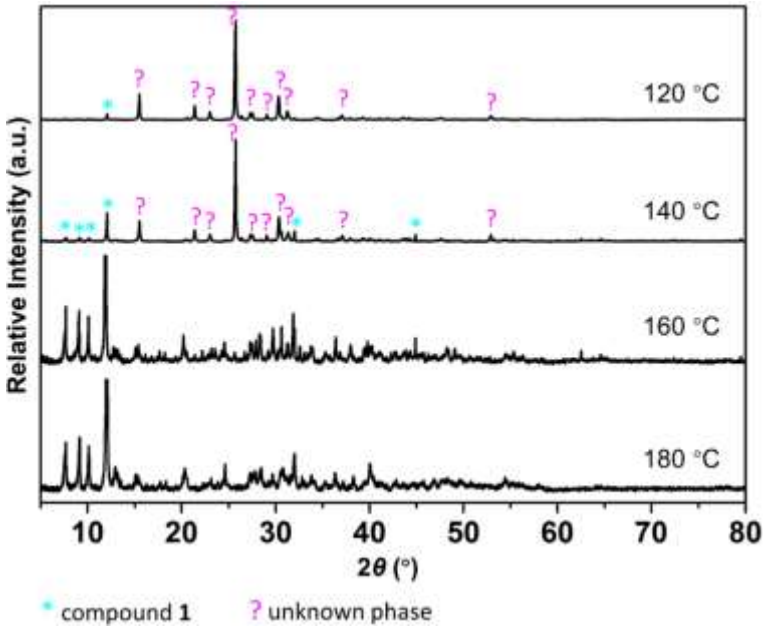

Figure S5. Powder XRD patterns for the products obtained from the optimizing reactions for **1** performed at different temperatures. The molar ratio of $N_2H_4 \cdot H_2O$:urea for all the reactions is 0.58:1.

Compound 2:

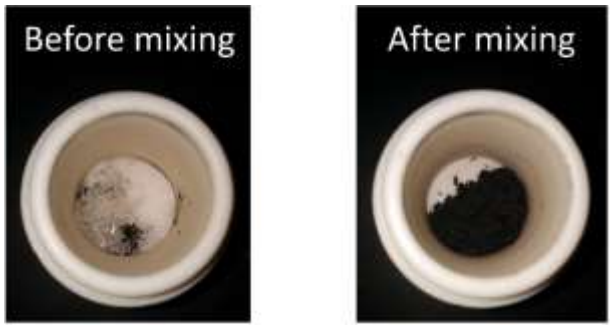

Figure S6. Photographs of the reactants, i.e. Sn, Se, $[NH_3CH_2CH_3]Cl$, urea (without $N_2H_4{\cdot}H_2O$), before and after being mixed for the synthesis of compound **2**. The transforming from bulk solid reactants to a viscous liquid mixture after being stirred indicates the formation of $[NH_2(CH_3)_2]Cl$-urea DES.

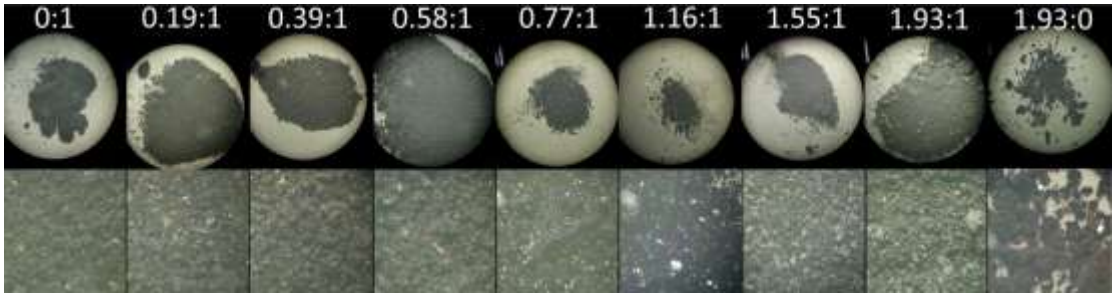

Figure S7. Photographs of the products obtained from the optimizing reactions for **2** with different $N_2H_4{\cdot}H_2O$:urea molar ratios at 160 °C. Top line: products washed by distilled water; bottom line: magnified imaging of the products.

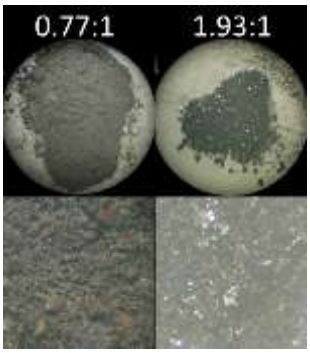

Figure S8. Photographs of the products obtained from the optimizing reactions for **2** at 160 °C in absence of $[NH_3CH_2CH_3]Cl$. The $N_2H_4{\cdot}H_2O$:urea molar ratios was tuned to 0.77:1 and 1.93:0 respectively. Top line: products washed by distilled water; bottom line: magnified imaging of the products.

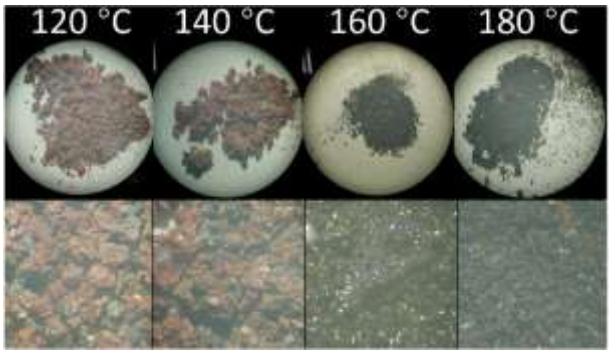

Figure S9. Photographs of the products obtained from the optimizing reactions for **2** ($N_2H_4 \cdot H_2O$:urea = 0.77:1) performed at different temperatures. Top line: products washed by distilled water; bottom line: magnified imaging of the products.

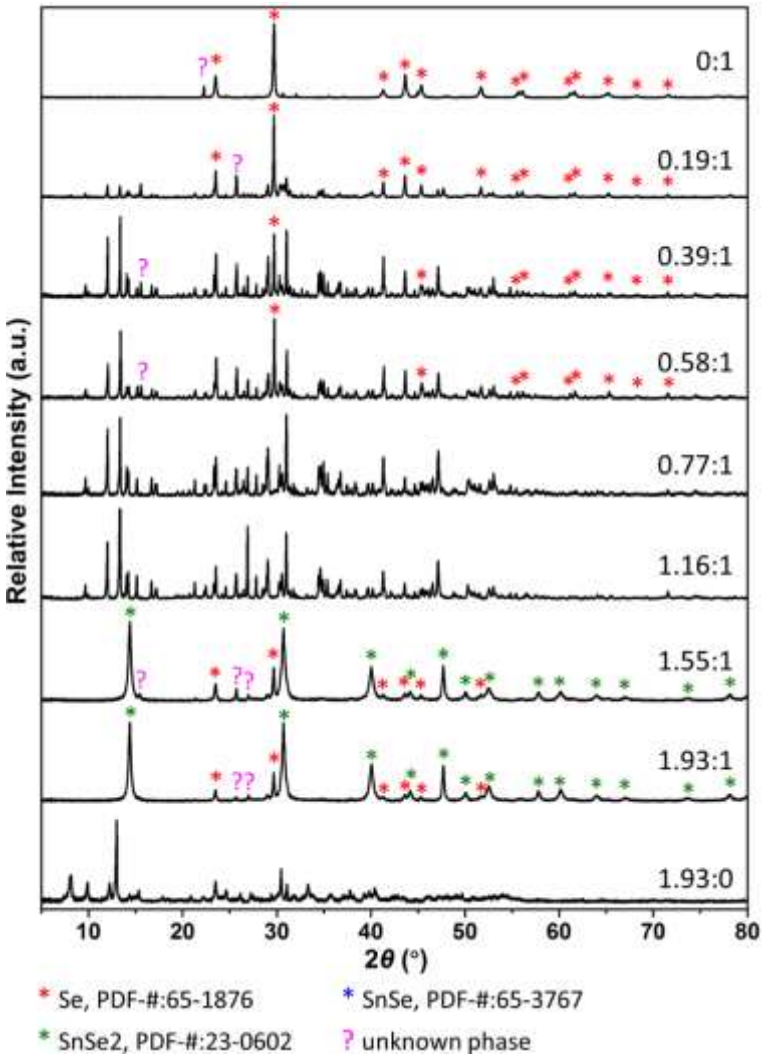

Figure S10. Powder XRD patterns for the products from optimizing reactions for **2** with different $N_2H_4 \cdot H_2O$:urea ratio at 160 °C.

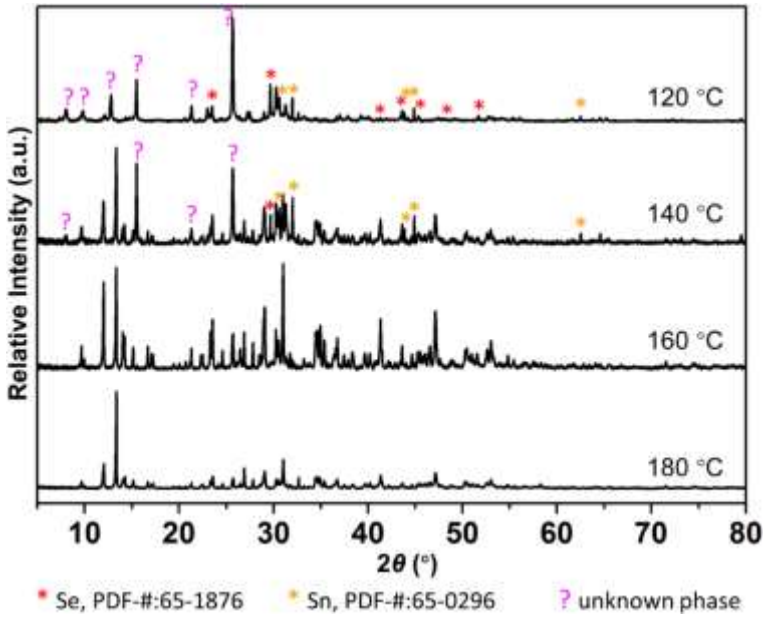

Figure S11. Powder XRD patterns for the products obtained from the optimizing reactions for **2** performed at 120-180 °C. The molar ratio of $N_2H_4 \cdot H_2O$:urea for all the reactions is 0.77:1.

Compound 4:

Figure S12. Photographs of the reactants, i.e. Sn, Se, $[NH(CH_3)_3]Cl$, urea (without $N_2H_4{\cdot}H_2O$), before and after being mixed for the synthesis of compound **4**. The transforming from bulk solid reactants to a viscous liquid mixture after being stirred indicates the formation of $[NH(CH_3)_3]Cl$-urea DES.

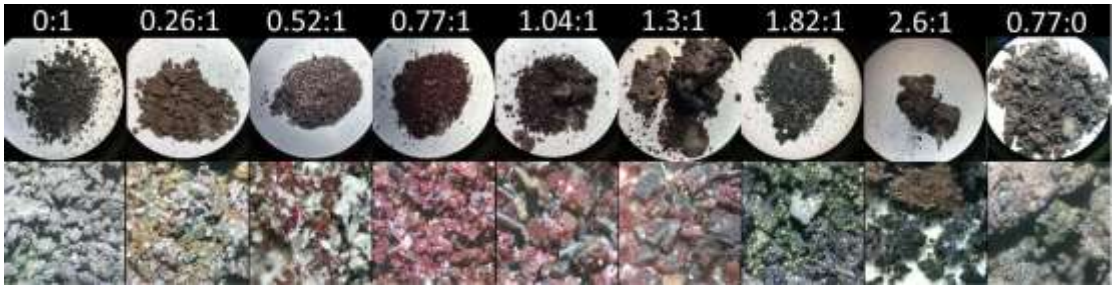

Figure S13. Photographs of the products obtained from the optimizing reactions for **4** with different $N_2H_4{\cdot}H_2O$:urea molar ratios at 160 °C. Top line: products washed by distilled water; bottom line: magnified imaging of the products.

Figure S14. Photographs of the products obtained from the optimizing reactions for **4** at 160 °C in absence of $[NH_3(CH_3)_3]Cl$. The $N_2H_4{\cdot}H_2O$:urea molar ratios was tuned to 0.77:1 and 1.3:0 respectively. Top line: products washed by distilled water; bottom line: magnified imaging of the products.

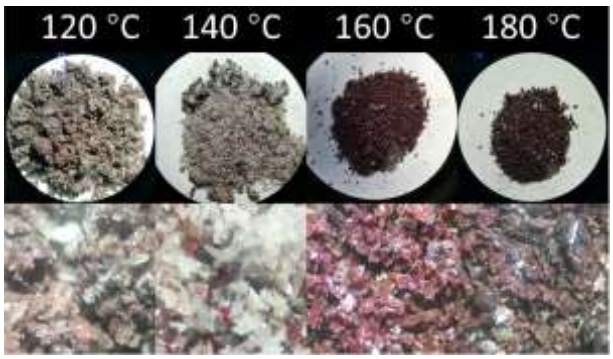

Figure S15. Photographs of the products obtained from the optimizing reactions for **4** ($N_2H_4 \cdot H_2O$:urea = 0.77:1) performed at different temperatures. Top line: products washed by distilled water; bottom line: magnified imaging of the products.

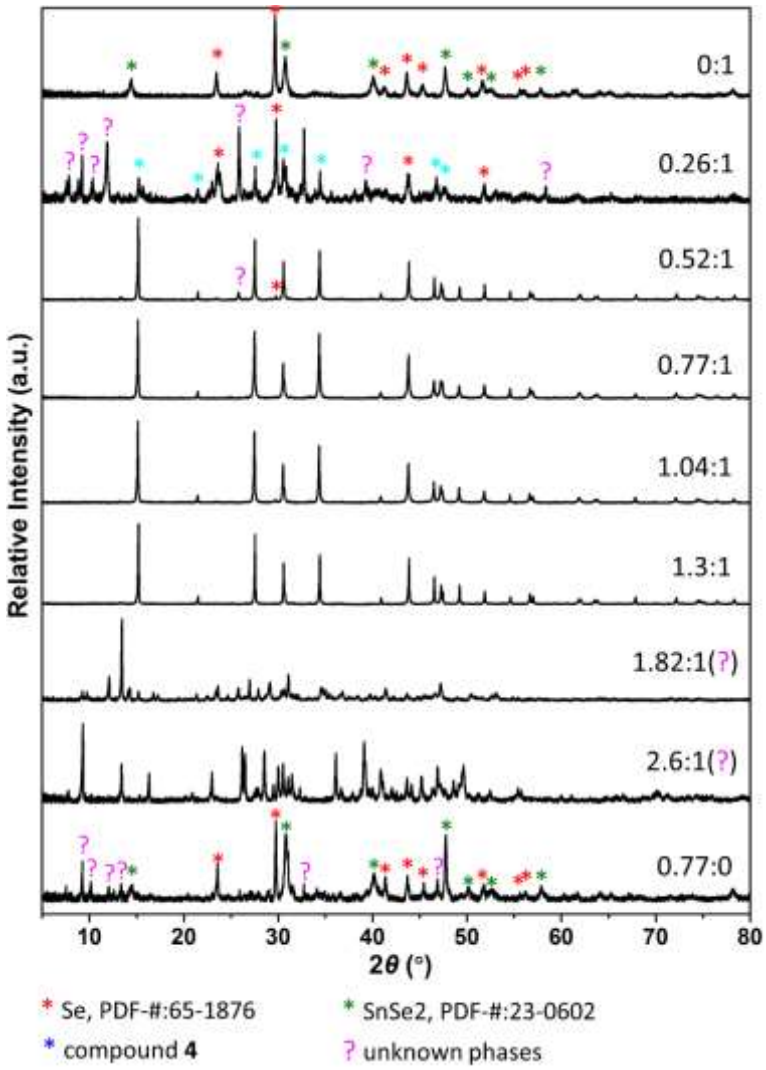

Figure S16. Powder XRD patterns for the products from optimizing reactions for **4** with different $N_2H_4 \cdot H_2O$:urea ratio at 160 °C.

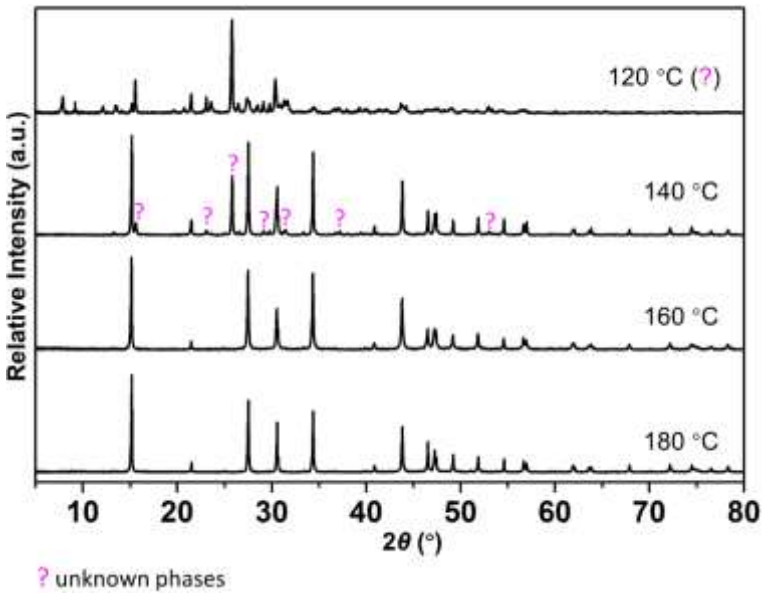

Figure S17. Powder XRD patterns for the products obtained from the optimizing reactions for **4** performed at 120-180 °C. The molar ratio of $N_2H_4 \cdot H_2O$:urea for all the reactions is 0.77:1.

2.2 Structures

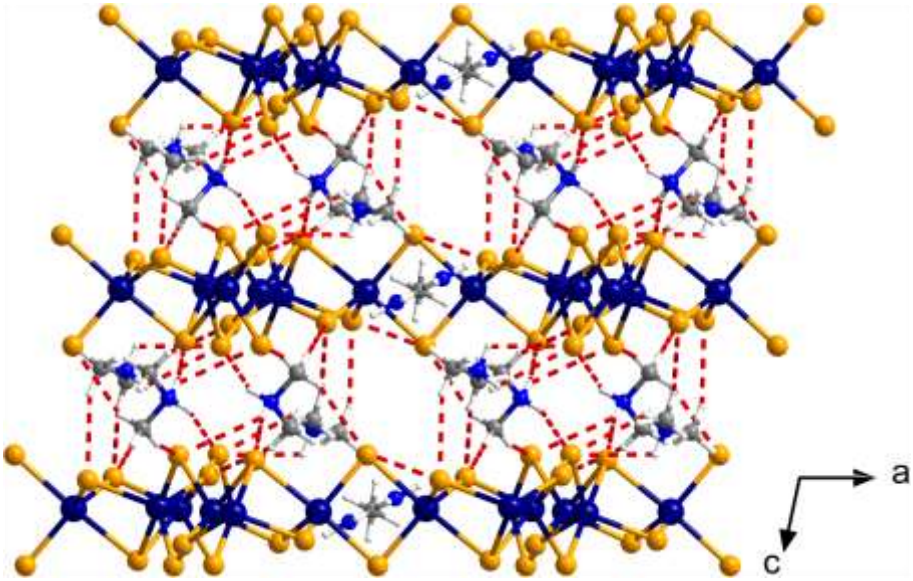

Figure S18. 3D supramolecular framework of **1** along the *b* axis (dashed lines represent the N−H···Se and C−H···Se hydrogen bonds). Color code: Sn (dark blue), Se (light orange), N (blue), C (gray), H (white).

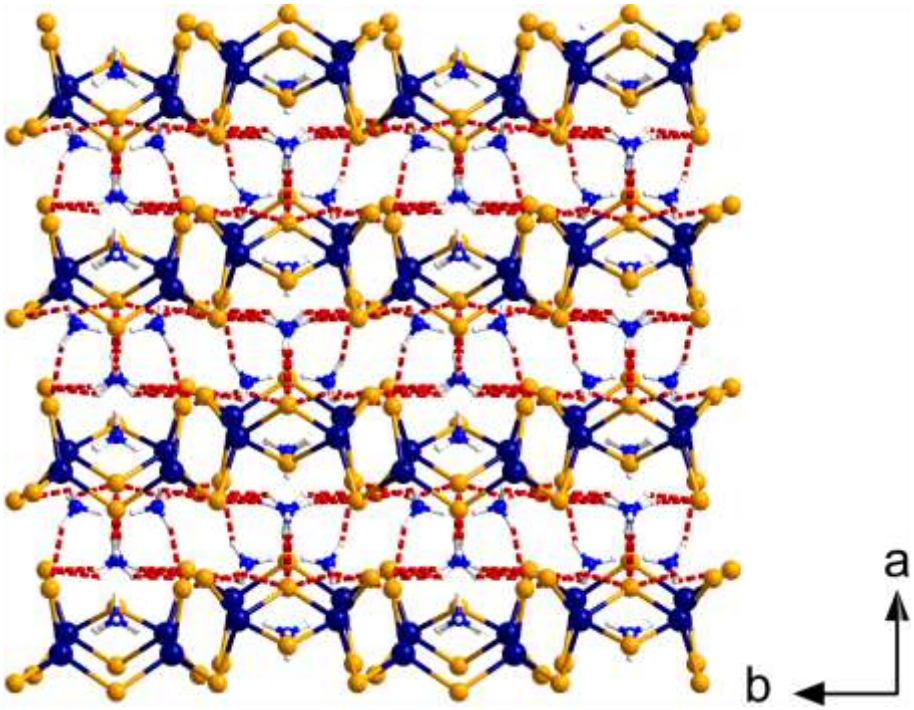

Figure S19. 3D supramolecular framework of **2** along the *c* axis (dashed lines represent the N−H···Se hydrogen bonds). Color code: Sn (dark blue), Se (light orange), N (blue), H (white).

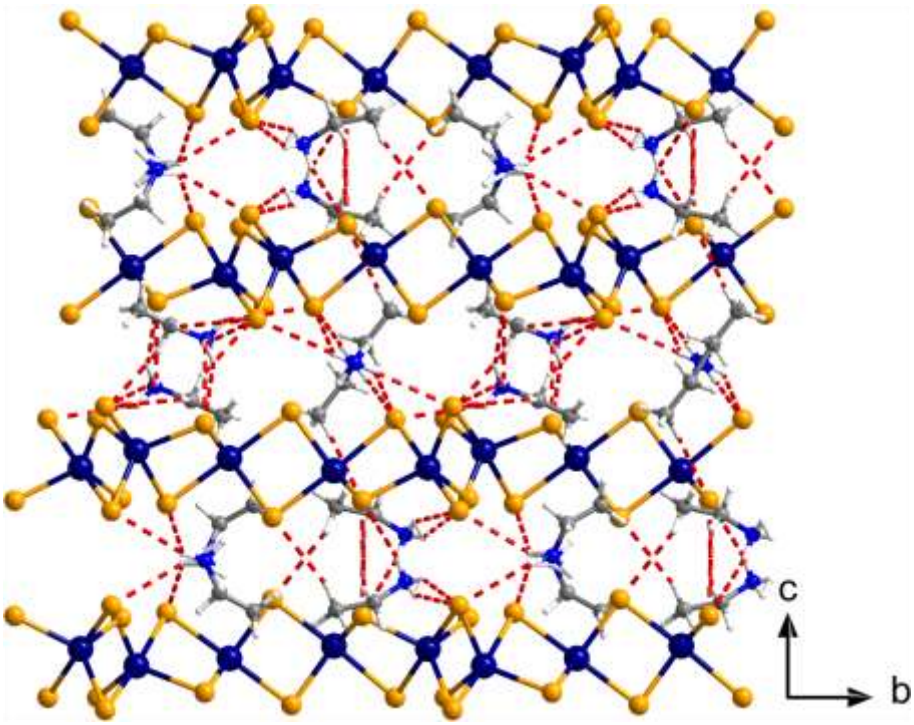

Figure S20. 3D supramolecular framework of **3** along the *a* axis (dashed lines represent the N−H···Se and C−H···Se hydrogen bonds). Color code: Sn (dark blue), Se (light orange), N (blue), C (gray), H (white).

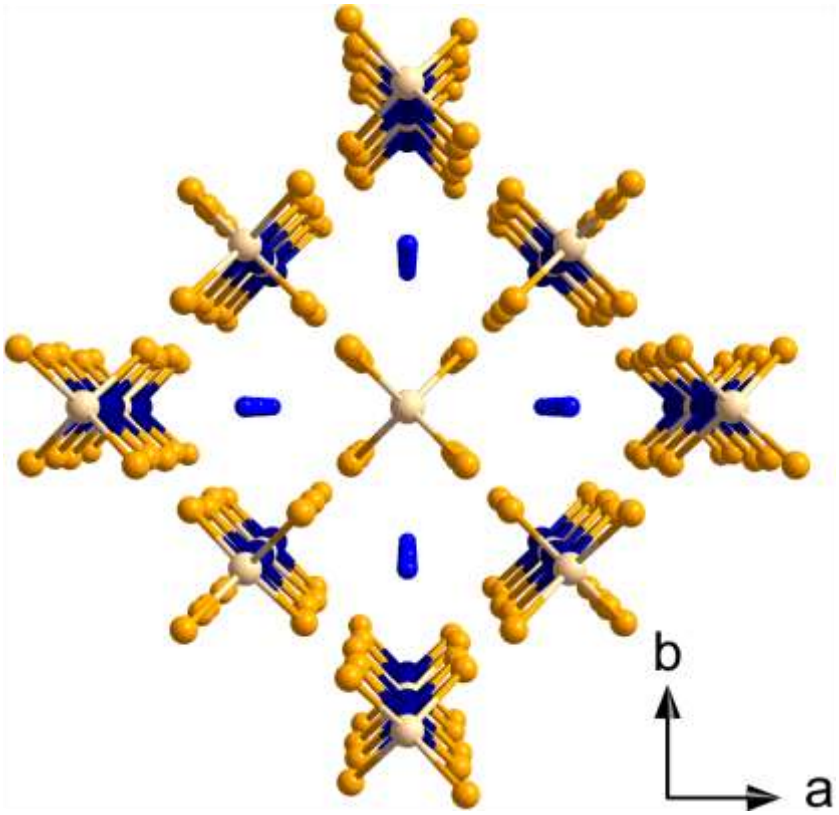

Figure S21. 3D supramolecular framework of **4** along the *c* axis. H atoms are omitted for clarity. Color code: Sn (dark blue), Ag (tan), Se (light orange), N (blue), C (gray).

2.3 Characterizations

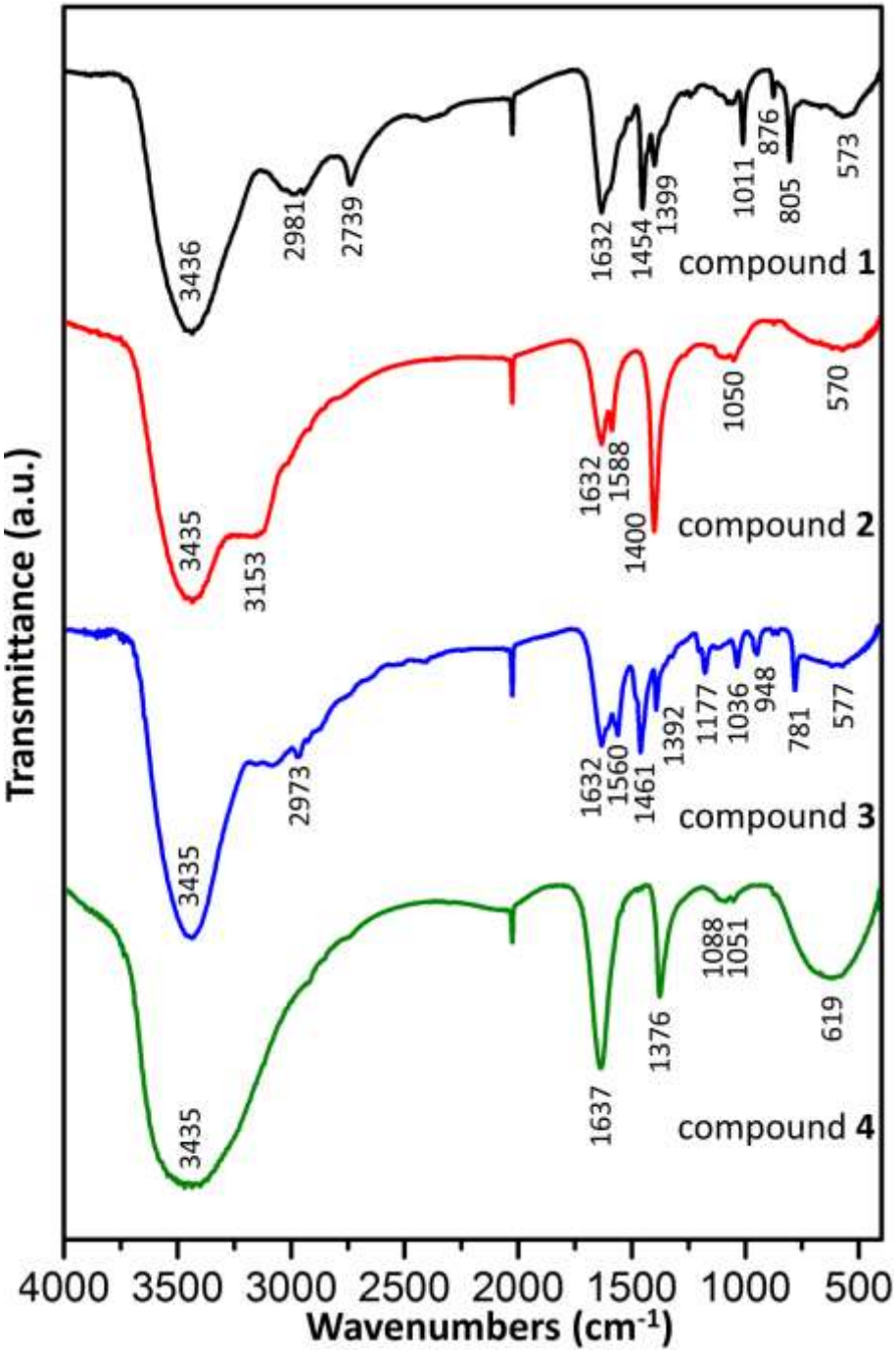

Figure S22. FTIR spectra of compounds **1**-**4** measured at room temperature on KBr pellets.

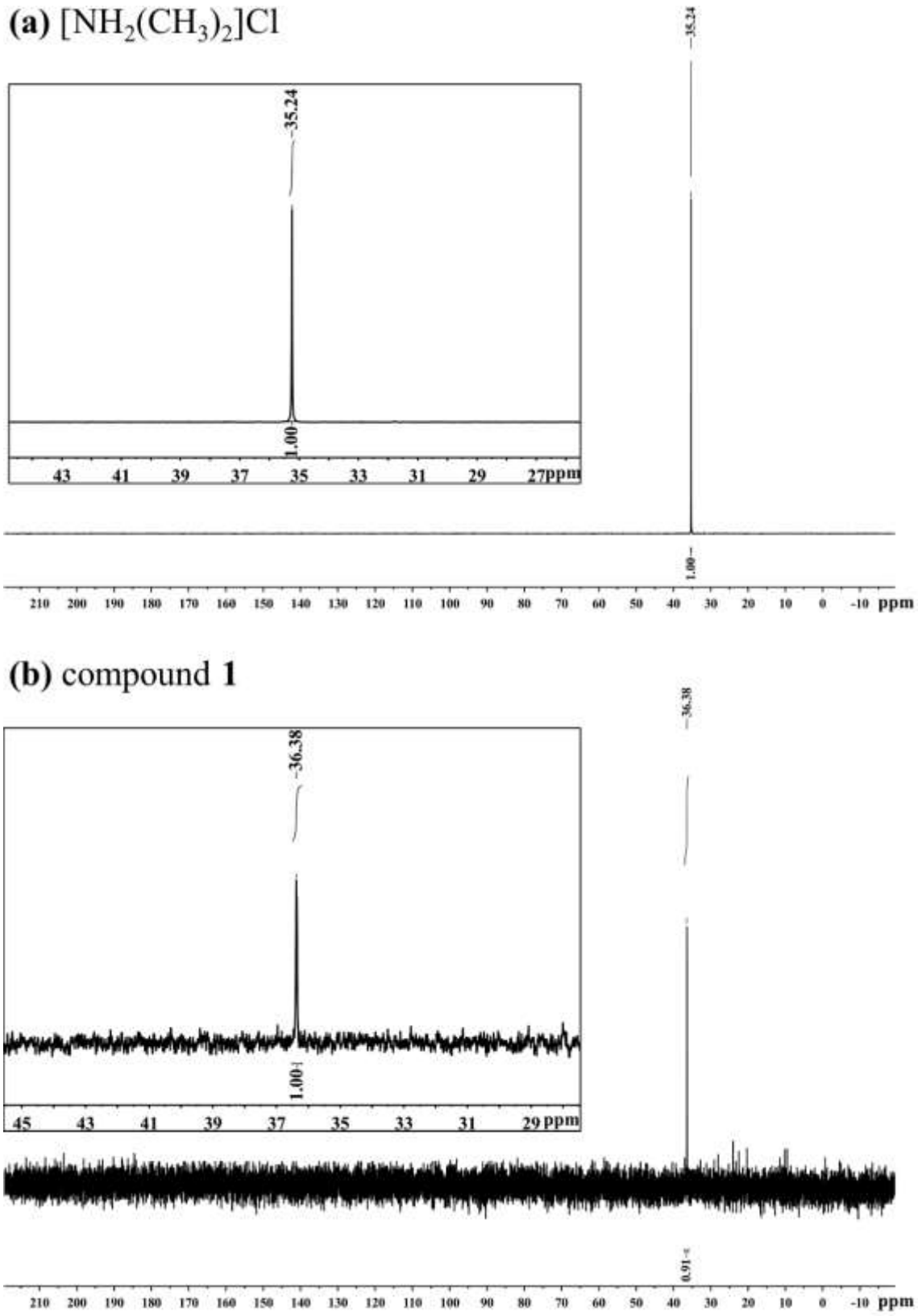

Figure S23. ^{13}C NMR spectra of (a) $[NH_2(CH_3)_2]Cl$ and (b) compound **1** dissolved in $N_2H_4 \cdot H_2O$ (98%)/D_2O recorded at room temperature.

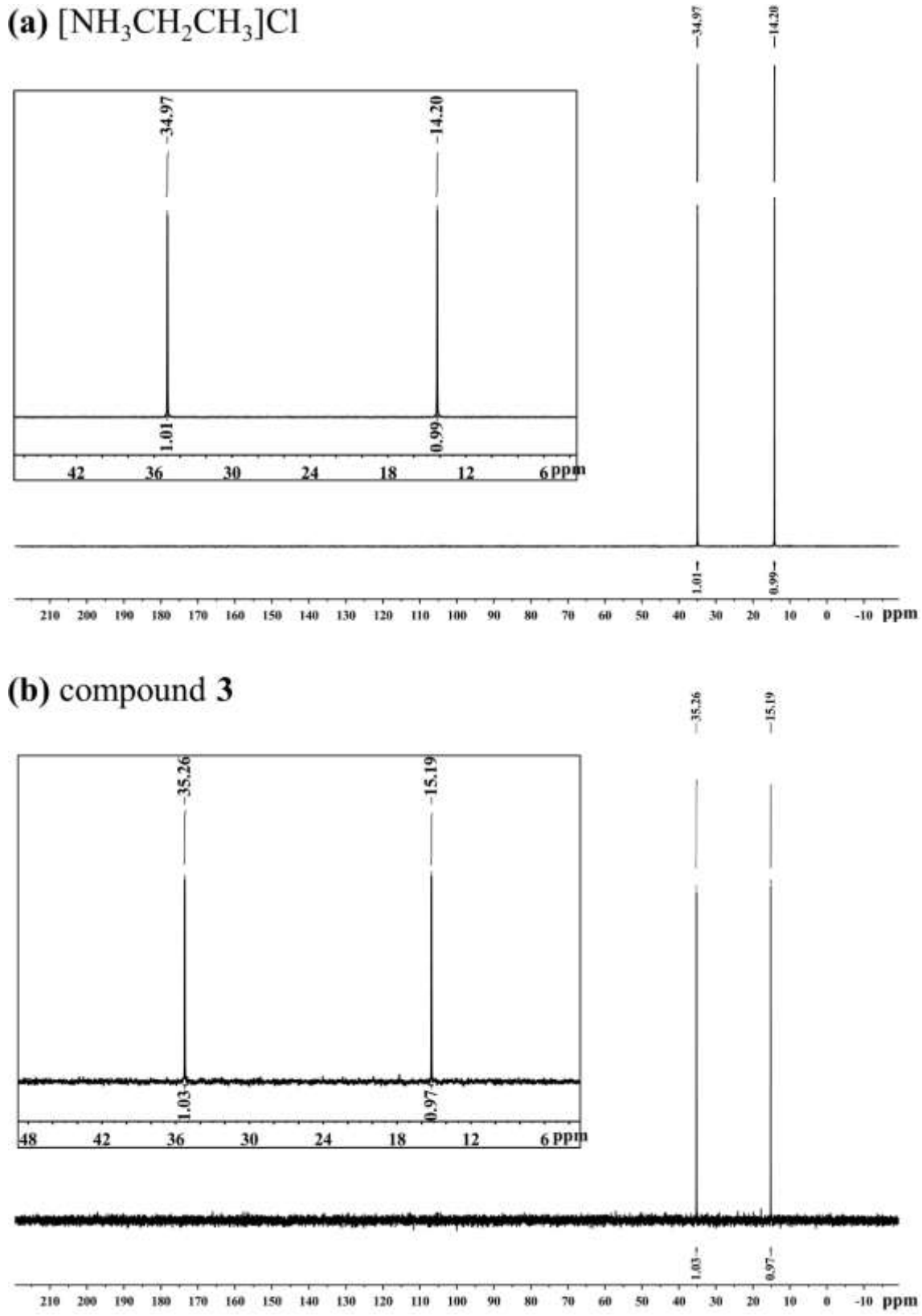

Figure S24. ^{13}C NMR spectra of (a) $[NH_3CH_2CH_3]Cl$ and (b) compound **3** dissolved in $N_2H_4 \cdot H_2O$ (98%)/D_2O recorded at room temperature.

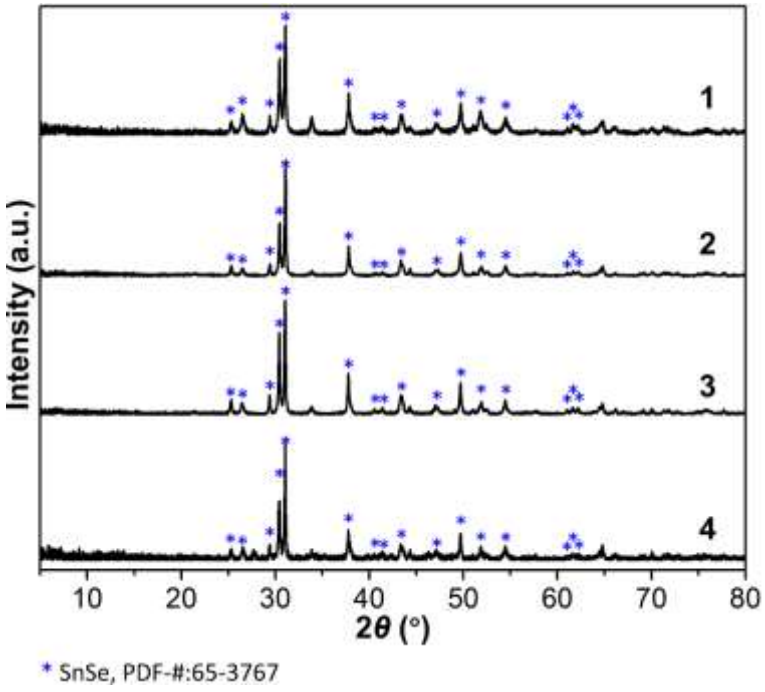

Figure S25. Powder XRD patterns for the TG residues of **1-4**.

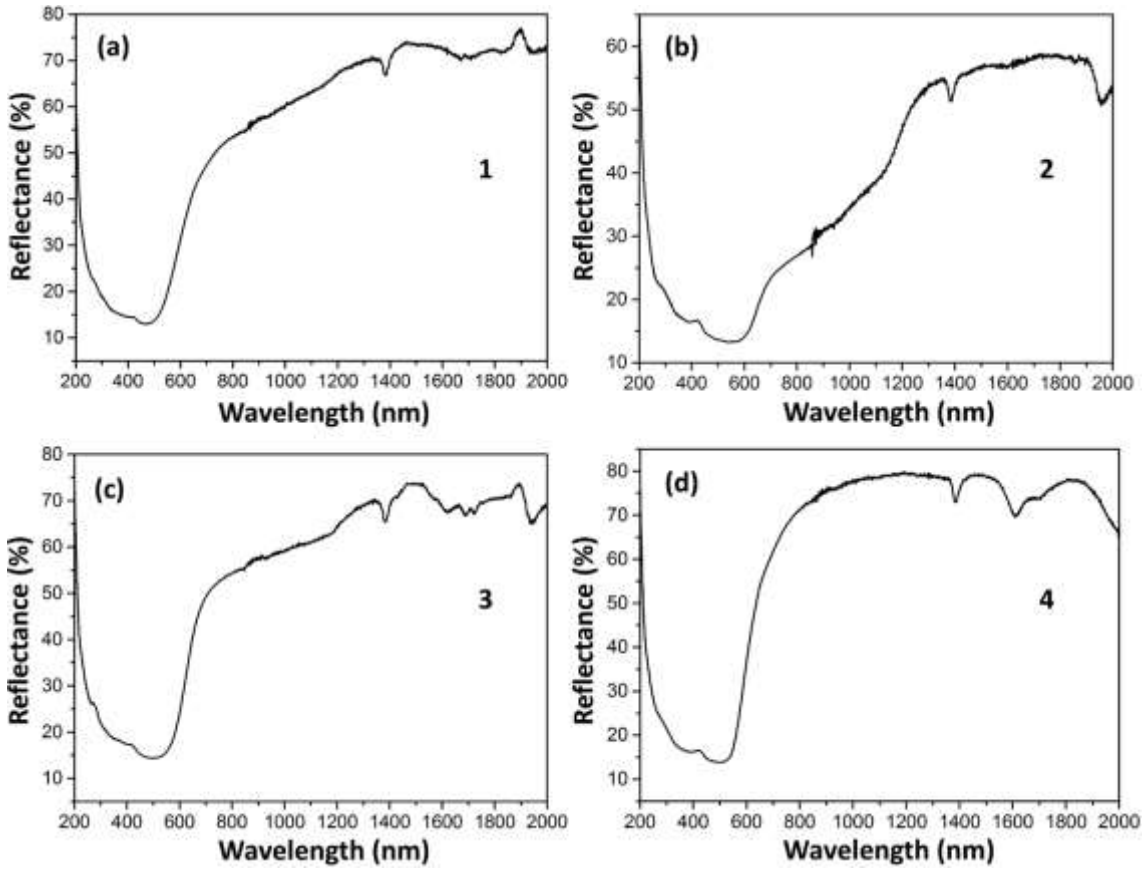

Figure S26. UV-vis reflectance spectra of compounds **1-4**.

References:

[1] W. S. Sheldrick, H.-G. Braunbeck, Preparation and crystal structure of $Cs_2Sn_3Se_7$, a cesium selenostannate(IV) with pentacoordinated Tin, *Z. Naturforsch. B* 1990, 45, 1643-1646.

[2] W. S. Sheldrick, H. G. Braunbeck, Preparation and crystal structure of ethylenediammonium selenostannates(IV) and $[2SnSe_2 \cdot en]_\infty$, *Z. Anorg. Allg. Chem.*1993, 619, 1300-1306.

[3] H. Aizari, G. A. Ozin, R. L. Bedard, S. Petrov, D. Young, Synthesis and Compositional Tuning of the Band Properties of Isostructural TMA-SnS_xSe_{1-x}-1 Nanoporous Materials, *Adv. Mater*. 1995, 7, 370-374.

[4] J. B. Parise, Y. Ko, K. Tan, D. M. Nellis, S. Koch, Structural evolution from tin sulfide (selenide) layered structures to novel 3- and 4-connected tin oxy-sulfides, *J. Solid State Chem.* 1995, 117, 219-228.

[5] A. Fehlker, R. Blachnik, Synthesis, structure, and properties of some selenidostannates. II. $[(C_2H_5)_3NH]_2Sn_3Se_7 \cdot 0.25H_2O$ und $[(C_3H_7)_2NH_2]_4Sn_4Se_{10} \cdot 4H_2O$, *Z. Anorg. Allg. Chem.* 2001, 627, 1128-1134.

[6] S. Lu, Y. Ke, J. Li, S. Zhou, X. Wu, W. Du, Solvothermal synthesis and structure of two 2D tin-selenides with long alkyldiamine $NH_2(CH_2)_nNH_2$ (n = 8, 10), *Struc. Chem.* 2003, 14, 637-642.

[7] G.-H. Xu, C. Wang, P. Guo, Poly[[(pentaethylenehexamine)manganese(II)] [hepta-μ-selenido-tritin(IV)]]: a tin–selenium net with remarkable flexibility, *Acta Cryst. C* 2009, 65, m171-m173.

[8] G.-N. Liu, G.-C. Guo, M.-J. Zhang, J.-S. Guo, H.-Y. Zeng, J.-S. Huang, Different effects of a cotemplate and $[(\text{transition-metal})(1,10\text{-phenanthroline})_m]^{2+}$ (m = 1-3) complex cations on the self-assembly of a series of hybrid selenidostannates showing combined optical properties of organic and inorganic components, *Inorg. Chem.* 2011, 50, 9660-9669.

[9] J.-R. Li, W.-W. Xiong, Z.-L. Xie, C.-F. Du, G.-D. Zou, X.-Y. Huang, From selenidostannates to silver-selenidostannate: structural variation of chalcogenidometallates synthesized in ionic liquids, *Chem. Comm.* 2013, 49, 181-183

[10] W.-W. Xiong, J. Miao, K. Ye, Y. Wang, B. Liu, Q. Zhang, Threading chalcogenide layers with polymer chains, *Angew. Chem. Int. Ed.* 2015, 54, 546-550.

[11] J. Lu, Y. Shen, F. Wang, C. Tang, Y. Zhang, D. Jia, Solvothermal syntheses and characterizations of selenidostannate salts of transition metal complex cations: conformational flexibility of the lamellar $[Sn_3Se_7^{2-}]_n$ Anion, *Z. Anorg. Allg. Chem.* 2015, 641, 561-567.

[12] S. Santner, S. Dehnen, $[M_4Sn_4Se_{17}]^{10-}$ cluster anions (M = Mn, Zn, Cd) in a Cs^+ environment and as ternary precursors for ionothermal treatment, *Inorg. Chem.* 2015, 54, 1188-1190.

[13] C.-F. Du, J.-R. Li, M.-L. Feng, G.-D. Zou, N.-N. Shen, X.-Y. Huang, Varied forms of lamellar $[Sn_3Se_7]_n^{2n-}$ anion: the competitive and synergistic structure-directing effects of metal-amine complex and imidazolium cations, *Dalton Trans.* 2015, 44, 7364-7372.

[14] D. D. Hu, Y. Y. Zhang, H. J. Yang, J. Lin, T. Wu, Structural transformation of selenidostannates from 1D to 0D and 2D via a stepwise amine-templated assembly strategy, *Dalton Trans.* 2017, 46, 7534-7539.

[15] K.-Y. Wang, D. Ding, S. Zhang, Y. Wang, W. Liu, S. Wang, S.-H. Wang, D. Liu, C. Wang,

Preparation of thermochromic selenidostannates in deep eutectic solvents, *Chem. Commun.*, 2018, 54, 4806-4809.

[16] K.-W. Kim, M.-Y. Heo *Z. Kristallogr.-New Cryst. Struct.* **2018**, 233, 255-257.

[17] X. Chen, X. Y. Huang, A. H. Fu, J. Li, L.-D. Zhang, H.-Y. Guo *Chem. Mater.*, 2000, **12**, 2385-2391.

[18] H. Guo, Z. Li, L. Yang, P. Wang, X. Huang, J. Li *Acta Crystallogr. C*: *Cryst. Struct. Commun.*, 2001, **57**, 1237-1238.

[19] L. D. Gulay, I. D. Olekseyuk, O. V. Parasyuk *J. Alloys Compd.*, 2002, **339**, 113-117.

[20] A. Assoud, N. Soheilnia, H. Kleinke *Chem. Mater.*, 2005, **17**, 2255-2261.

[21] M. Daszkiewicz, L. D. Gulay, A. Pietraszko, V. Y. Shemet *J. Solid State Chem.*, 2007, **180**, 2053-2060.

[22] M. Ji, M. Baiyin, S. Ji, Y. An *Inorg. Chem. Commun.*, 2007, **10**, 555-557.

[23] H. G. Yao, R.-C. Zhang, S.-H. Ji, M. Ji, Y. L. An, G. L. Ning *Inorg. Chem. Commun.*, 2010, **13**, 1296-1298.

[24] J.-R. Li, X.-Y. Huang, *Dalton Trans.*, 2011, **40**, 4387-4390.

[25] J.-R. Li, W.-W. Xiong, Z.-L. Xie, C.-F. Du, G.-D. Zou, X.-Y. Huang, *Chem. Commun.*, 2013, **49**, 181-183.

[26] K.-Z. Du, X.-H. Qi, M.-L. Feng, J.-R. Li, X.-Z. Wang, C.-F. Du, G.-D. Zou, M. Wang, X.-Y. Huang *Inorg. Chem.*, 2016, **55**, 5110-5112.

[27] B. Zhang, M.-L. Feng, J. Li, Q.-Q. Hu, X.-H. Qi, X.-Y. Huang *Cryst. Growth Des.*, 2017, **17**, 1235-1244.